Impact of obstacles on dislocation patterning and stress correlations

J. M. Rickman,[1,*] M. Haataja,[2,3,†] and R. LeSar[4,‡]
[1]*Department of Materials Science and Engineering and Department of Physics, Lehigh University, Bethlehem, Pennsylvania 18015, USA*
[2]*Department of Mechanical and Aerospace Engineering, Princeton University, Princeton, New Jersey 08540, USA*
[3]*Princeton Institute for the Science and Technology of Materials (PRISM), Princeton University, Princeton, New Jersey 08540, USA*
[4]*Department of Materials Science and Engineering, Iowa State University, Ames, Iowa 50011, USA*
(Received 11 June 2007; revised manuscript received 18 December 2007; published 6 May 2008)

By virtue of their long-ranged nature, elastic stresses due to dislocations may provide a mechanism for the spatial organization of alloys with misfitting constituents. Here, we first explore the connection between dislocation patterning and correlations in elastic stress fields associated with dislocations. Specifically, we examine the impact of obstacles, such as impurities and grain boundaries, on the pattern formation in a collection of mutually interacting dislocations. This is accomplished by characterizing the order in terms of various dislocation structure factors that reflect the tendency to form dislocation wall segments. We find that random stationary impurities frustrate wall formation without altering the characteristic length scale of the dislocation patterning, while grain boundaries promote wall formation via dislocation incorporation, and frustrate polygonization away from the boundaries. We then discuss the implication of the results of induced solute patterning in phase-separating alloys.

DOI: 10.1103/PhysRevB.77.174105 PACS number(s): 61.72.Lk, 07.05.Tp

I. INTRODUCTION

From the materials physics perspective, the presence of dislocations in both metals and semiconductors is associated with elastic strain fields that alter their mechanical and electrical responses and lead to patterning at various scales.[1] In this context, patterning may involve the extended networks formed by dislocation self- organization, such as those occurring in heavily worked metals,[2,3] or other structures that were induced from an energetically preferred arrangement of dislocations. The energetic and kinematic factors that control such a pattern formation have been discussed in several studies.[4–6] An example of induced patterning occurs in semicoherent and heteroepitaxial semiconducting films, wherein the elastic strain associated with misfit dislocations promotes spinodal decomposition during deposition, and therefore self-patterning via the resulting spatial periodicity.[7,8] Furthermore, there are suggestions that misfit dislocations can also facilitate pattern formation in first-order phase transitions by modifying the nucleation and growth kinetics in a transforming thin film.[8]

One of the characteristic features of dislocation stress fields is that they are long ranged. Specifically, for straight lines, the magnitude of the stress field decays in the same way as $1/r$, where r denotes the distance from the dislocation core.[1] These stress fields in turn can induce ordering in objects that have an associated eigenstrain. Consider, for example, a well-worked metallic alloy in which the coupling of alloy composition to the elastic field of dislocations can give rise to a compositional patterning.[7,9] In particular, it is of interest to determine whether or not ordering exists in the ground state of an alloy given a spatially extended dislocation substructure. In this case, the stress associated with the dislocation substructure will vary from region to region, and it is sensible to regard the (hydrostatic) dislocation stress field coupling to the alloy composition as a random external field.

Physical systems affected by random fields have a long history. From a theoretical perspective, perhaps the best studied case is that of the random field Ising model (RFIM), wherein the spins on a lattice are coupled to a spatially varying external magnetic field. Typically, for simplicity, the disorder is taken to be spatially uncorrelated and drawn from the Gaussian distribution of a given width or from a bimodal distribution. In their classic paper, Imry and Ma[10] argued that for the two-component vector spins, the presence of disorder prevents long-ranged order from developing in dimensions $d \leq 4$, while for scalar spins the critical dimension is two. It was later rigorously shown that the ground state is disordered in two spatial dimensions for any finite disorder strength,[11] while in three spatial dimensions, long-ranged order persists up to a critical disorder strength at low temperatures.[12] Additionally, long-ranged isotropic correlations in the disorder was considered in the past.[13,14] As will be shown below, however, in the case of dislocations, the correlations in the effective disorder are typically both long ranged and anisotropic, and it is of interest to investigate (a) how such correlations arise and (b) how they are reflected in the alloy ground states. Both topics will be addressed in this paper.

Given these considerations, we examine here those factors that affect dislocation pattern formation and, in particular, we assess the role that various obstacles (e.g., impurities and grain boundaries) play in the formation of those dislocation wall arrangements that lead to a reduction in the system energy. For this purpose, we employ Monte Carlo simulation methods to generate relaxed substructures for straight edge dislocations. A simplified, two-dimensional dislocation model is used here to illustrate the generic features of dislocation and/or obstacle interactions that affect patterning. Systems consisting of dislocations that have Burgers vectors of both same and different signs are considered. In these simulations, we also incorporate stationary impurities and low-angle grain boundaries, with the latter as an array of immobile dislocations. To quantify the wall ordering in these

structures, both partial and total structure factors are defined as averages over an ensemble of dislocation configurations. The structure factors are then linked by considering spatial correlations in relaxed structures. We note that similar correlations were recently examined for like-signed dislocations in two dimensions with no obstacles.[15]

This paper is organized as follows: In Sec. II, a short outline of the Monte Carlo simulation methodology is presented and the assumptions regarding defect interactions are summarized. In Sec. III, the results of the simulations are given for systems containing obstacles and grain boundaries. Section IV contains a discussion of the results and their implications for compositional patterning in phase-separating binary alloys.

II. SIMULATION METHODOLOGY

Our discussion of dislocation pattern formation in the presence of obstacles begins with an energetic model that is employed to generate relaxed defect configurations. Consider a collection of M straight edge dislocations, each with a Burgers vector $\vec{b}=\pm b\hat{x}$ $(b>0)$ and a line direction $\hat{\ell}=\hat{z}$, and M_{imp} impurities distributed at random on the sites of a two-dimensional, spatially periodic $L\times L$ square lattice such that double occupancy is forbidden. It is assumed that these objects are embedded in an elastically isotropic medium that have a shear modulus μ and a Poisson ratio ν. The motion of a given dislocation is confined to a single slip plane, namely, its starting plane $y=$constant (i.e., climb is disallowed), and the impurities are taken to be immobile obstacles with zero misfit. Grain boundaries are modeled as arrays of immobile dislocations oriented along the y axis with M_{dis} dislocations per boundary.[16] Given the long-ranged anisotropic interactions between edge dislocations in this medium, upon relaxation these line defects tend to organize into walls to lower the stored elastic energy. As will be seen below, the presence of impurities and grain boundaries frustrate polygonization by blocking possible relaxation pathways. It is noteworthy that such two-dimensional dislocation simulations have been employed in the past to elucidate dislocation pattern formation under an external stress[17–20] as well as to develop coarse-grained dislocation descriptions.[21–23]

A relaxed configuration for this system can be obtained via a zero-temperature Monte Carlo (MC) simulation as follows: (1) a mobile dislocation is selected at random, (2) a move is attempted in which the mobile dislocation is placed at a randomly selected neighbor site in the same slip plane, and (3) the move is accepted if the new site contains neither a dislocation nor an impurity and if the overall energy of the system E_{TOT} does not increase, i.e., $\Delta E_{\text{TOT}}\leq 0$. These steps are repeated until the energy converges, which in most cases happens after a few hundred time units. As customary, the time unit in a simulation is the Monte Carlo step (MCS), which is defined as the increment in which each dislocation has the opportunity to move once on average. For convenience, we take b, the lattice parameter, and $\pi\mu/(1-\nu)$ to be unity. We note that other simulation procedures,[15,17,24] including, for example, Langevin dynamics, can also be employed to generate relaxed structures.

For simplicity, it is assumed here that there is no misfit strain, and hence, no elastic interaction associated with the impurities. The energy required in the MC simulation can thus be calculated from the interaction energy between a reference dislocation located at the origin and another located at (x,y), along with its periodic images. These images can be regarded as a series of infinite walls with each wall parallel to the y axis comprising dislocations separated by L lattice sites. The interaction energy between the reference dislocation and a single wall is given by[15,25]

$$E(x,y) = -\frac{\mu b^2}{4\pi(1-\nu)}\left\{\ln\{\cosh(2\pi\bar{x})-\cos(2\pi\bar{y})\} - \frac{2\pi\bar{x}\sinh(2\pi\bar{x})}{\cosh(2\pi\bar{x})-\cos(2\pi\bar{y})}+\ln 2\right\}, \tag{1}$$

where $\bar{x}=x/L$ and $\bar{y}=y/L$ are scaled coordinates. Thus, to obtain the total interaction energy for the reference dislocation, one calculates

$$E_{\text{int}}(x,y) = \sum_{n=-s}^{n=+s} E(x-nL,y), \tag{2}$$

where, in practice, the wall index s can be truncated at about seven cells owing to the rapid convergence of the sum in Eq. (2). In order to obtain the change in the total energy of the system ΔE_{TOT}, E_{int} is computed for all dislocation pairs in the system involving the reference dislocation, both before and after the attempt. It should be noted that since the impurities have zero misfit strain, their presence does not affect the elastic energy of the system. Since the impurities are immobile, they serve, however, to block dislocation motion.

Here, our focus is on the order associated with a dislocation ensemble in which each element of the ensemble is a relaxed configuration generated from a different random initial condition by using the procedure outlined above. Several investigators have characterized spatial order in these systems by using weighted pair correlation functions as well as tools appropriate for cluster analyses.[26–28] A useful and related probe of the spatial order in this system is the dislocation density correlation function and related quantities. In particular, if an edge dislocation α is located at the position $\vec{R}_\alpha$, the total dislocation density tensor has a nonzero component $\rho_{zx}(\vec{r})=\Sigma_{\alpha=1}^{M} b_\alpha \delta(\vec{r}-\vec{R}_\alpha)$, where the subscripts z and x denote the line direction and Burgers vector direction, respectively, and where, from the discussion above, $b_\alpha=\pm 1$. Thus, it is convenient to define a static structure factor[29]

$$S(\vec{q}) = \frac{1}{M}\langle\rho_{zx}(\vec{q})\rho_{zx}(-\vec{q})\rangle = \frac{1}{M}\Big\langle\sum_{\alpha=1}^{M}\sum_{\beta=1}^{M} b_\alpha b_\beta \exp[i\vec{q}\cdot(\vec{R}_\alpha-\vec{R}_\beta)]\Big\rangle, \tag{3}$$

where the angle brackets denote the aforementioned ensemble average. If an equal number of dislocations having

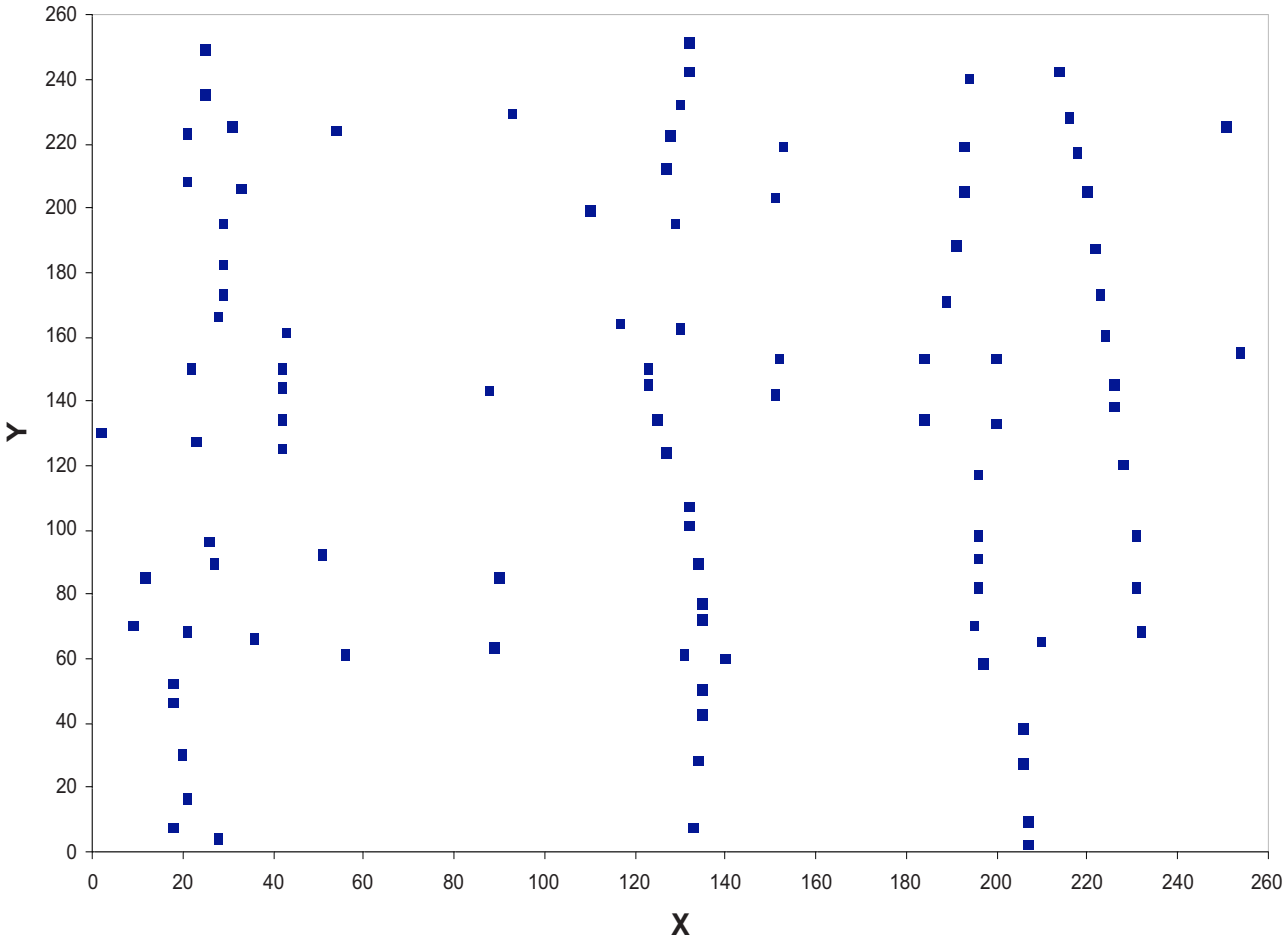

FIG. 1. (Color online) A relaxed configuration comprising $M=100$ positive edge dislocations in the absence of impurities. Note the tendency to form wall segments.

both positive and negative Burgers vectors is present, one can regard this as a two-component system and write, in terms of the partial structure factors $S^{++}(\vec{q})$, $S^{--}(\vec{q})$, and $S^{+-}(\vec{q})$,[30,31]

$$S(\vec{q}) = S^{++}(\vec{q}) + S^{--}(\vec{q}) - (S^{+-}(\vec{q}) + S^{-+}(\vec{q})). \quad (4)$$

These correlation functions will be employed below to characterize spatial ordering in relaxed defect structures.

III. SIMULATION RESULTS

The various simulations described below were performed on an $L \times L$ square lattice, which ranged in size from $L=32$ to $L=256$, on which M edge dislocations are initially distributed at random. To assess the impact of the dislocation density on our results, several different values in the range from $M=50$ to $M=400$ were employed here.

A. Effects of impurities on dislocation ordering

We begin by considering the energetics of this system in the presence of randomly distributed impurities when all dislocations have a positive Burgers vector. For a given initial state, the system is evolved for 300–400 MCS, which is a sufficient number of iterations in this case needed to obtain a relaxed configuration. A typical final configuration for $M=100$ that highlights dislocation polygonization that results in multiple wall segments in the absence of impurities is shown in Fig. 1. This procedure is then repeated for 500–2000 different initial conditions and the results are averaged over these independent runs. It is found that the relaxed energy considerably varies from run to run as the constrained energy minimization results in trapping in the local minima.

It is useful to first obtain a descriptor that reveals spatial correlations among dislocation wall segments. This information is contained in the wall correlation function, $S(q_x, q_y=0)$, where $q_y=0$ implies an integration in real space over the dislocation content of a wall oriented parallel to the y axis. Figure 2(a) shows the wall correlation function as a function of $\bar{q}=q_x L/2\pi$ for a collection of positive edge dislocations with $M=100$ and $M_{\text{imp}}=0$. Note the presence of a clear peak in the correlation function. The height of the peak is determined by the number of dislocations per wall segment (as well as the overall dislocation density), and the peak position reveals a characteristic length scale $L/\bar{q} \approx 50$ in the system. In real space, this length corresponds to the end of a denuded zone wherein the local dislocation density is low (i.e., a trough in the pair correlation function[15]). To highlight the dependence of the scale of ordering on dislocation density, Fig. 2(b) shows the wall correlation function versus $\bar{q}$ (at

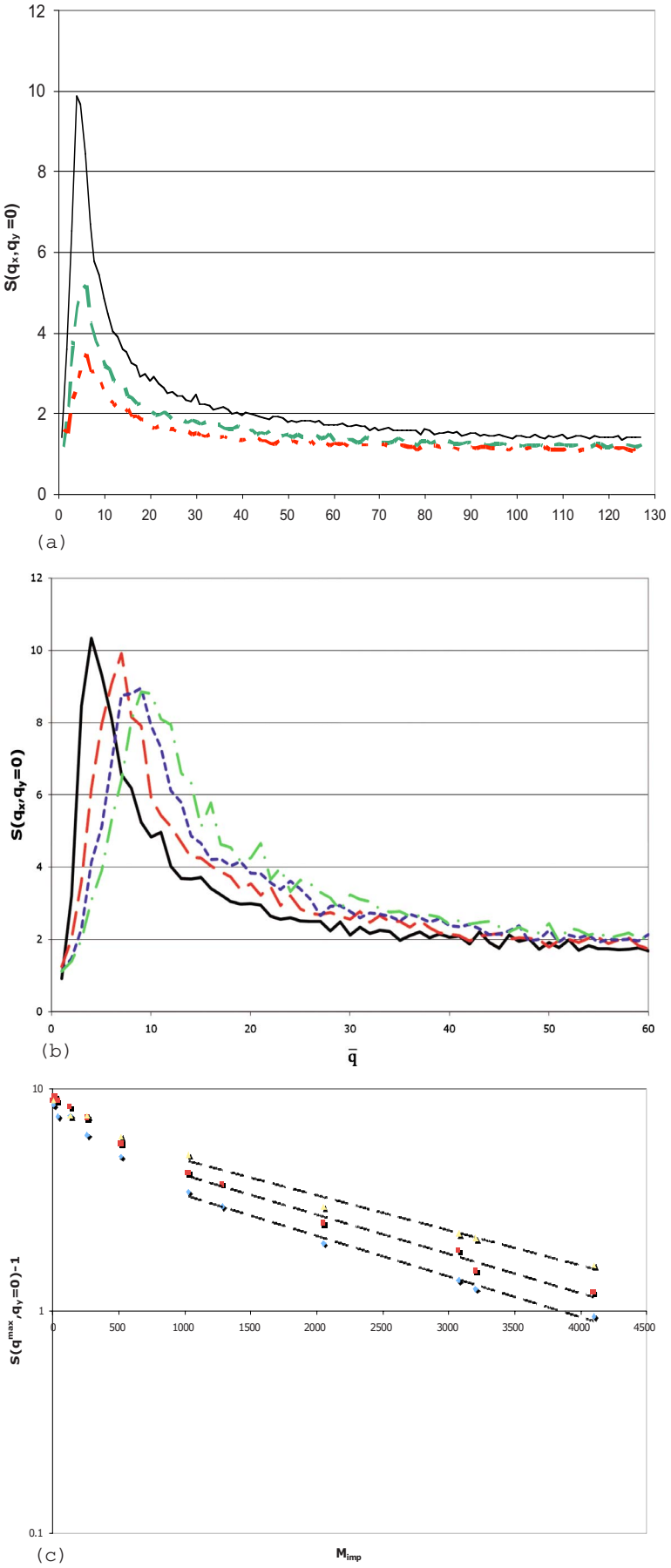

FIG. 2. (Color online) (a) The wall correlation function, $S(q_x, q_y=0)$, as a function of normalized wave vector, $\bar{q}=q_x L/2\pi$, for $M=100$ with impurity fractions $f=M_{\mathrm{imp}}/L^2=0.0$ (upper curve), 0.016 and 0.031 (lower curve). The results represent an average over 1000 independent runs. In each case, the location of the peak is insensitive to the impurity level and sets a length scale for dislocation patterning. The decrease in peak height associated with an increase in impurity concentration indicates that wall formation is frustrated. (b) The wall correlation function versus $\bar{q}$ (at relatively large $\bar{q}$) for $M=100$ (solid line, leftmost peak), 200 (dashed line), 300 (dotted line), and 400 (dashed-dotted line) (rightmost peak), respectively. (c) $S(q^{\max}, q_y=0)-1$ versus M_{imp} for randomly distributed impurities for $M=50$ ($\diamond$), 100 ($\square$), and 200 ($\triangle$), respectively. For large M_{imp}, the data were fit to the exponential function $S(q^{\max}, q_y=0)-1=\exp(-f\pi r_c^2)$. The effective radii were found to be $r_c=2.97$, 2.92, and 2.76 lattice parameters, respectively, with an error of approximately 0.1 lattice parameters.

relatively large $\bar{q}$) for a range of dislocation densities in the absence of impurities. The shift in peak position to higher values of $\bar{q}$ that is associated with an increase in dislocation density indicates a decreasing interwall spacing, as expected. We note that the location of the peak was also examined for $L=32$, 64, and 128 at a fixed dislocation density. For this range of system sizes, it was found that the peak position is relatively insensitive to L, which suggests that the scale of the pattern depends on the reduced dislocation coordinates $\vec{R}/L$.

As also shown in Fig. 2(a) are the wall correlation functions that correspond to $f=M_{\mathrm{imp}}/L^2=0.016$ and 0.031 for $M=100$. As evident from Fig. 2(a), an increase in the impurity content of the system leads to a decrease in the peak height, with essentially no shift in peak position, implying less ordering at the same scale. The impact of impurity concentration on ordering, as embodied in the peak height of the wall correlation function $S(q^{\max},q_y=0)-1$ (where $q^{\max}$ is the peak location for a given impurity concentration), for a range of dislocation and impurity concentrations is shown in Fig. 2(c) for $M=50$, 100, and 200. These results are consistent with the expectation that impurities inhibit wall formation by blocking relaxation pathways. If other pathways were added by, for example, allowing climb, this impurity effect would be mitigated. We note that similar results were found in the study by Thomson *et al.*[15] In that case, there were no impurities, but they examined the ordering within walls as a function of dislocation density, i.e., the dislocations served as a set of moving obstacles. They found that the ordering within the walls scaled as an inverse power of the dislocation density—the more "obstacles" in the system there are, the less ordering within the walls there is.

The results displayed in Fig. 2(c) can be more quantitatively understood by considering the factors governing wall formation. A particular dislocation can join a wall if it can move unimpeded from its initial position to a wall location. As a function of impurity concentration, the fraction of the semi-free dislocations is approximately given by the probability p that a stationary, randomly distributed impurity will not be encountered within some effective radius r_c. For a Poisson process, one expects that $p=\exp(-f\pi r_c^2)$, where r_c, like the interwall separation, is a function of M. As evident from Fig. 2(c), this relation accurately describes the behavior of the wall correlation function for each M after some initial regime as determined by the dislocation spacing. The effective radii were found to be $r_c=2.97$, 2.92, and 2.76 lattice parameters. The small decrease in r_c upon increasing M implies that the average distance that a dislocation travels to join a wall decreases as expected. Clearly, the mobility of a dislocation is also determined by the location of other dislocations, and so, one would expect that this exponential dependence on f would roughly break down when the average spacing for randomly distributed dislocations is nearly that for the average impurity spacing (i.e., when $M\approx M_{\mathrm{imp}}$). The results in Fig. 2(c) indicate that the crossover from the initial to the exponential regime occurs at somewhat smaller average impurity spacings, which is a consequence in part of the long-range nature of dislocation-dislocation interactions.

The presence of both positive and negative dislocations leads to a more complex ordering involving dislocation dipoles. The observed structures result from an interplay among factors that favor the wall and dipole formation. A typical relaxed structure for a collection of $M=100$ positive and negative edge dislocations (thus having no net Burgers vector) with an initial random distribution on the lattice is shown in Fig. 3. As evident from Fig. 3, dipolar arrangements, some as part of the wall segments, form at the favored 45° orientations.

As in the example above, one can probe the tendency to polygonize by calculating wall functions, both for dislocations of the same sign and for the entire collection. In the former case, the relevant correlation function is given in terms of the average partial structure factor $(S^{++}(q_x,q_y=0)+S^{--}(q_x,q_y=0))/2$, as shown in Fig. 4. (For this system $S^{++}=S^{--}$.) As before, the peak location in this correlation function reflects an underlying length scale in the dislocation patterning, while the peak height indicates a lesser propensity for a wall formation relative to that in a system comprising only the positive edge dislocations.

Also shown in Fig. 4 is the total wall correlation function $S(q_x,q_y=0)$. Its shape can be rationalized as follows: If the system entirely consisted of dipoles, then one could assign to the location of each positive dislocation i a displacement vector $\vec{u}_i$ to the location of a negative dislocation. For simplicity, if one then assumes that the displacement is independent of i and follows a circularly symmetric Gaussian distribution with standard deviation α, one would have, approximately, that

$$S(\vec{q}) \approx 2S^{++}(\vec{q})(1-e^{-1/2\alpha^2q^2}). \tag{5}$$

Thus, the peak in the partial structure factor is damped by a q-dependent coefficient that arises from the spatial correlations between dislocations of opposite sign. The situation here is somewhat more complex since dipole formation is incomplete owing to the tendency to form walls (see Fig. 3).

B. Effects of grain boundaries on dislocation ordering

Next, consider the impact of grain boundaries on dislocation pattern formation. For simplicity, the focus here will be on one or more low-angle grain boundaries, as modeled by fixed dislocation arrays along the y axis. The nature of the obstacle and/or mobile dislocation interaction here is somewhat more complex owing to the interaction between the grain boundary and the mobile dislocations set by the spacing of the dislocations comprising the boundary (i.e., the misorientation). As a result, while some dislocations are repelled by the boundary, others are incorporated to lower the system energy. This trapping of formerly mobile dislocations by the grain boundary impedes the relaxation of other dislocations impinging on the boundary.

The wall correlation function is again a revealing probe of the tendency to polygonize. Figure 5(a) shows $S(q_x,q_y=0)$ versus $\bar{q}$ for a system containing $M=100$ mobile positive edge dislocations and a single boundary containing a fraction $g=M_{\mathrm{dis}}/L^2=1.22\times10^{-4}$ of immobile dislocations. Similar to the impurity results outlined above, the decrease in peak height that attends to an increase in g indicates that the grain-boundary dislocations and those that are trapped at the

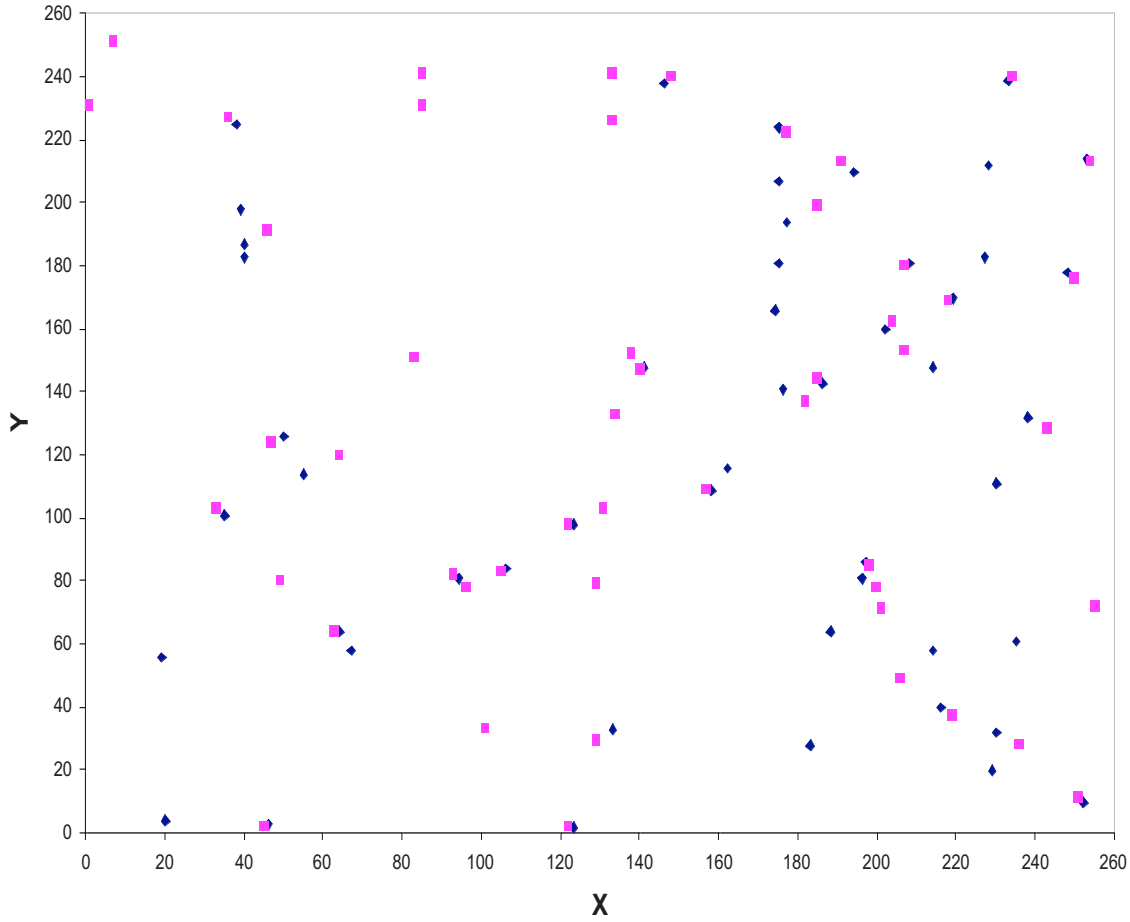

FIG. 3. (Color online) A relaxed configuration comprising $M=100$ positive and negative edge dislocations (with no net Burgers vector) in the absence of impurities. Note the tendency to form wall segments and dipoles.

boundary inhibit wall formation without changing the inherent length scale of the patterning. This frustration of wall formation overall occurs despite the incorporation of dislocations into grain boundaries. Indeed, it was found that the average number of dislocations trapped at the boundary increased until about $M_{\mathrm{dis}}=32$, with the subsequent decrease in the rate of addition primarily owing to the lack of available empty boundary sites.

By contrast, a new length scale can be set via the introduction of a series of boundaries, as shown in Fig. 5(b). More specifically, as evident from Fig. 5(b), a crude polycrystal consisting of a series of grain boundaries separated by $L/4$, each containing 16 dislocations, leads to a qualitatively different structure factor. Peaks in the wall correlation function at $\bar{q}=4\beta$ (where β is an integer) result from the incorporation of some dislocations into the grain boundaries and peaks at a high wave number suggest that the confining effect of the grain boundaries leads to correlations at shorter length scales.

IV. DISCUSSION

In this work, the impact of obstacles, such as impurities and grain boundaries, on the pattern formation in a collection of mutually interacting dislocations was investigated by using Monte Carlo simulation methods. It was found that the presence of immobile impurities hindered dislocation polygonization without significantly altering the underlying length scale of the substructure. By contrast, the presence of grain boundaries was found to promote wall formation via the incorporation of mobile dislocations into a grain boundary while also frustrating dislocation wall formation away from grain boundaries.

These findings have direct relevance to the behavior of phase-separating alloys in two spatial dimensions. In particular, misfitting solute atoms directly couple to the hydrostatic stress field present in the system.[7,9] If one adopts a lattice spin model to describe the local composition in an alloy,[32] the RFIM[10] can be invoked to assess the tendency for compositional ordering in the ground state in such alloys. Here, it is the spatial dependence of the dislocation stress-stress correlation function that is the key in determining the presence (or lack thereof) of an ordered ground state structure. Specifically, extended domains wherein the local hydrostatic stress has a given sign (associated with long-ranged stress correlations) will favor domains of one of the phase-separated alloy phases, resulting in an ordered structure. On the other hand, if the stress correlations are short ranged (i.e., asymptotically delta functions), we expect the domains to fragment as in the standard RFIM picture. Finally, if the stress correlation function oscillates around zero at short

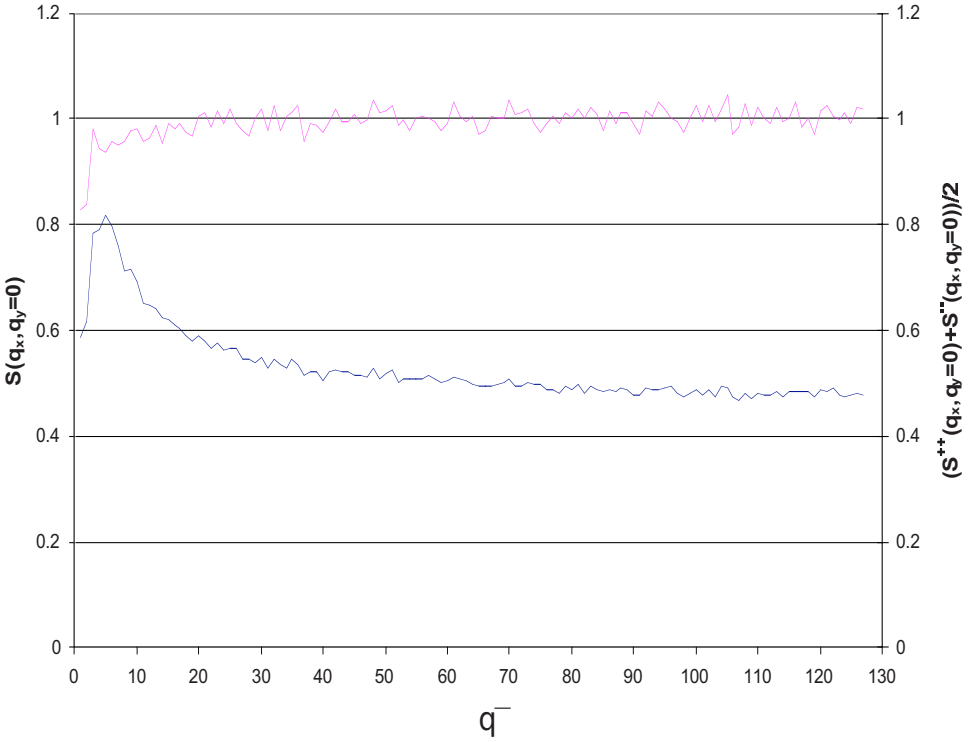

FIG. 4. (Color online) The wall correlation function, $S(q_x, q_y=0)$ (upper curve) and the average partial structure factor, $(S^{++}(q_x, q_y=0)+S^{--}(q_x, q_y=0))/2$, as a function of normalized wave vector, $\bar{q}$, for the systems that have both positive and negative edge dislocations. The results represent an average over 2000 independent runs. The peak height in the partial structure factor indicates a lesser propensity for wall formation relative to a system containing only positive edge dislocations.

scales, we expect local compositional patterning to take place, provided that the coupling to the hydrostatic stress field is sufficiently strong. In particular, the coupling must at least balance the excess free energy of the compositional interfaces associated with local patterning. In the following, we will investigate the behavior of the stress correlation function in terms of the dislocation structure factor and then draw conclusions regarding possible compositional patterning within different scenarios for the spatial dislocation distributions.

For a collection of edge dislocations in two spatial dimensions in which $\vec{b}=\pm b\hat{x}$ $(b>0)$ and $\hat{\ell}=\hat{z}$, dislocation stresses can be obtained from the Airy stress function χ via $\sigma_{xx}=-\partial^2\chi/\partial y^2$, $\sigma_{yy}=-\partial^2\chi/\partial x^2$, and $\sigma_{xy}=\partial^2\chi/\partial x\partial y$, where χ satisfies[9]

$$\nabla^4\chi=-Y_2\sum_j b_j\nabla_y\delta(\vec{r}-\vec{r}_j), \tag{6}$$

where Y_2 denotes the two-dimensional Young's modulus. Upon Fourier transform, the hydrostatic stress becomes

$$\hat{\sigma}_{ii}(\vec{q})=-q^2\hat{\chi}(\vec{q})=-\frac{iY_2q_y}{q^2}\sum_j b_j\exp(i\vec{q}\cdot\vec{r}_j) \tag{7}$$

for $\vec{q}\neq 0$ and $\hat{\sigma}_{ii}(\vec{q}=0)=0$; the latter follows from the observation that the hydrostatic stress field of an isolated edge dislocation in two spatial dimensions integrates to zero in an infinite system. Hence, the relevant correlation function here is[33]

$$\langle\hat{\sigma}_{ii}(\vec{q})\hat{\sigma}_{jj}(-\vec{q})\rangle=\frac{MY_2^2q_y^2}{q^4}S(q_x,q_y), \tag{8}$$

where $\hat{\sigma}_{ij}(\vec{q})$ are the components of the dislocation stress tensor in Fourier space. Thus, the tendency for compositional ordering is directly related to the behavior of the dislocation structure factor. In the discussion below, we will consider a few special cases.

Let us begin with M dislocations with $b_x=b$, which are uniformly randomly distributed. This arrangement corresponds to the starting configuration for the collection of positive edge dislocations that is considered in Sec. III. It is easy to show that, in this case, $S^{\text{rand}}(q_x,q_y)=b^2+(M-1)b^2\delta_{\vec{q},0}$. Hence, the stress correlation function simply becomes

$$\langle\hat{\sigma}_{ii}(\vec{q})\hat{\sigma}_{jj}(-\vec{q})\rangle=\frac{Mb^2Y_2^2q_y^2}{q^4} \tag{9}$$

for $\vec{q}\neq 0$ and $\langle\hat{\sigma}_{ii}(\vec{q}=0)\hat{\sigma}_{jj}(-\vec{q}=0)\rangle=0$. The inverse Fourier transform of the expression in Eq. (9) is both anisotropic and long ranged in real space due to the $\sim q^{-2}$ dependence at small $\vec{q}$, implying that macroscopic domains are favored by the random field, and hence, no dislocation-induced compositional patterning occurs. This is consistent with numerical results in Ref. 7, wherein it was shown that the role of stationary and randomly distributed dislocations in a system that undergoes spinodal decomposition was mainly to serve as localized seeds for the initial composition waves without affecting late-time coarsening behavior.

In the case of correlations among the dislocations, we may consider the following phenomenological expression, which is consistent with the numerically obtained structure factor in the presence of randomly distributed obstacles:

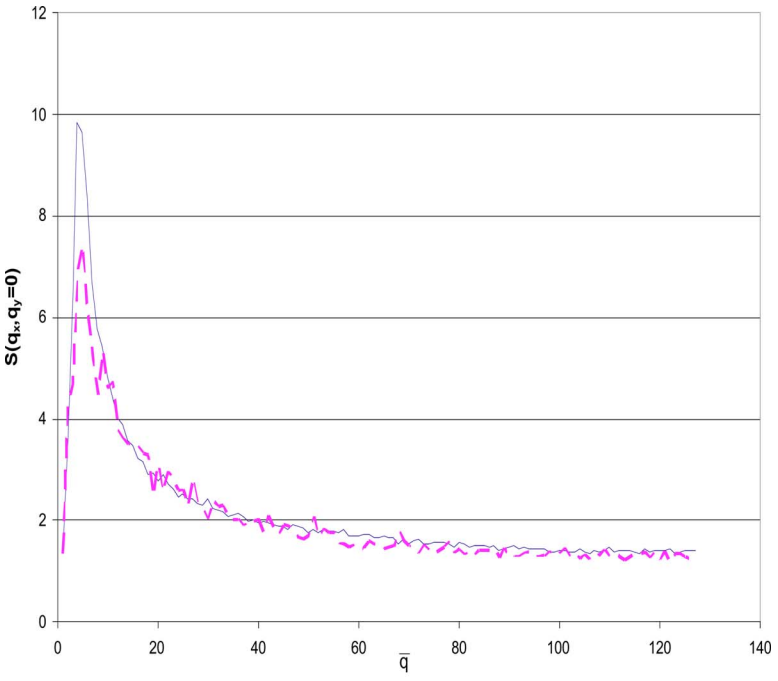

(a)

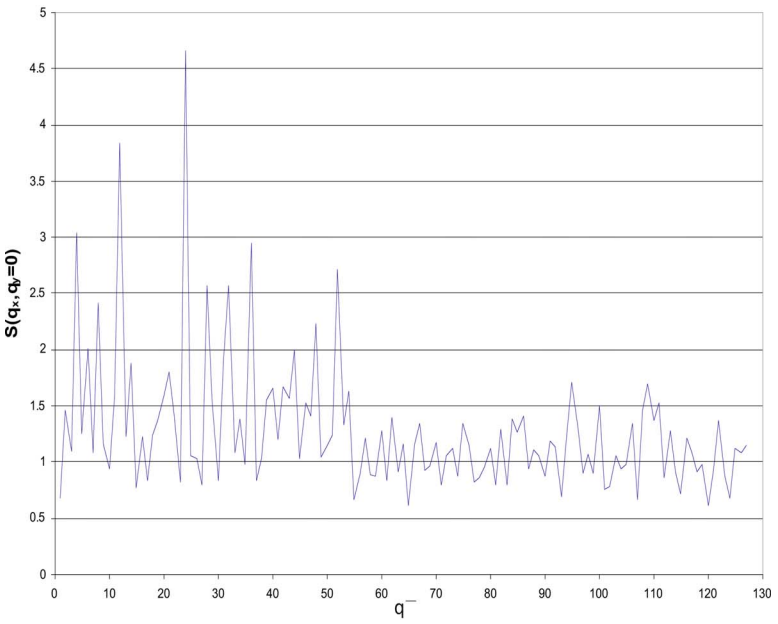

(b)

FIG. 5. (Color online) (a) The wall correlation function, $S(q_x, q_y=0)$, as a function of normalized wave vector, $\bar{q}$ for a single grain boundary with $g=0.0$ (upper curve) and $g=1.22\times10^{-4}$. The results were averaged over 1500 independent runs. (b) The same as (a) except that there are multiple walls spaced at a distance of $L/4$, with each wall containing 16 dislocations. The results were averaged over 2700 independent runs.

$$S(q_x,q_y) = \frac{(1-\alpha)b^2}{1+(q_x-q_{0;x})^2\xi_x^2+(q_y-q_{0;y})^2\xi_y^2} + \alpha b^2 + C\delta_{\vec{q},0}. \tag{10}$$

Here, α denotes the fraction of dislocations pinned by the obstacles and thus are unable to participate in wall formation, ξ_j denotes the correlation length in the jth direction, while $\sim q_{0;j}^{-1}$ corresponds to a preferred separation between dislocation aggregates, which is also in the jth direction. We set $\alpha=0$ for now and discuss the case $\alpha>0$ later. Physically, one can think of ξ_x as the mean dislocation pileup size, while ξ_y denotes the mean GB segment length. In this case, the stress correlation function becomes (for $\vec{q}\neq0$)

$$\langle\hat{\sigma}_{ii}(\vec{q})\hat{\sigma}_{jj}(-\vec{q})\rangle = \frac{Mb^2Y_2^2q_y^2}{q^4}\frac{1}{1+(q_x-q_{0;x})^2\xi_x^2+(q_y-q_{0;y})^2\xi_y^2}. \tag{11}$$

Consider collections of either finite-sized GB segment or pileups, which are otherwise uncorrelated. In the former case, we may set $\xi_y=\ell$, $\xi_x=0$, and $q_{0;y}=q_{0;x}=0$, while in the latter case $\xi_x=\ell$, $\xi_y=0$, and $q_{0;y}=q_{0;x}=0$. For these choices, the stress correlation function becomes

$$\langle \hat{\sigma}_{ii}(\vec{q})\hat{\sigma}_{jj}(-\vec{q})\rangle = \frac{Mb^2Y_2^2q_y^2}{q^4}\frac{1}{1+q_{0;x/y}^2\ell^2}. \quad (12)$$

In both cases, numerical evaluation of the resulting stress correlation function reveals that they are monotonically decreasing for $|\vec{r}-\vec{r}'|<L/2$ (and thus, long ranged), implying that no induced compositional patterning is expected.

Next, we consider the case of finite and spatially correlated GB segments and pileups. In the former case, we may set $\xi_y=\ell$, $\xi_x\neq 0$, and $q_{0;y}=0$ with $q_{0;x}=q_0$, while in the latter case $\xi_x=\ell$, $\xi_y\neq 0$, and $q_{0;x}=0$ with $q_{0;y}=q_0$. In both cases, sufficiently long-ranged correlations in the direction perpendicular to the dislocation aggregate give rise to a spatially oscillating stress correlation function, which implies patterning given a strong enough coupling. Specifically, we simply require that $\xi_x \gg q_0^{-1}$ in the GB case and $\xi_y \gg q_0^{-1}$ in the pileup case.

At this point, it is useful to consider the effect of obstacles on patterning. We recall that based on our simulation results, the main effect of the obstacles is to renormalize the peak height of the structure factor. This is equivalent to setting $\alpha>0$ in Eq. (10). As the fraction of dislocations pinned by the obstacles α increases, the magnitude of the stress oscillations decreases, leading to a disappearance of the compositional patterning beyond a critical impurity density.

Finally, for the case of infinite aggregate sizes, the stress correlation function vanishes for dislocation walls, while in the case of infinite pileups, it becomes

$$\langle \hat{\sigma}_{ii}(\vec{q})\hat{\sigma}_{jj}(-\vec{q})\rangle = \frac{Mb^2Y_2^2}{q_y^2}\frac{1}{1+(q_y-q_0)^2\xi_y^2}. \quad (13)$$

Now, if $\xi_y \gg q_0^{-1}$, the hydrostatic stress field oscillates around zero with a period $\sim q_0^{-1}$; thus, a compositional stripe pattern emerges for a sufficiently strong coupling between the composition and hydrostatic stress field due to dislocation pileups.

To summarize, in this paper, we have examined the formation of spatial structures in frustrated dislocation ensembles in two spatial dimensions and the implications thereof on compositional patterning in phase-separating alloys. Specifically, we have shown that immobile impurities interfere with dislocation wall formation and, thus, have a strong impact on compositional patterning. In closing, we hope that the work presented in this paper catalyzes new experimental and theoretical studies on the effects of partially-ordered and frustrated defect structures on phase transformations.

ACKNOWLEDGMENTS

The authors would like to thank the U.S. Air Force Office of Scientific Research for support under Grant No. FA9550-05-1-0082. This work was also supported in part by NSF-DMR Grant No. 0449184 (M.H.). R.L. gratefully acknowledges the support of Iowa State University.

*jmr6@lehigh.edu
†mhaataja@princeton.edu
‡lesar@iastate.edu

[1] J. Friedel, *Dislocations* (Pergamon, New York, 1964).
[2] D. A. Hughes, D. C. Chrzan, Q. Liu, and N. Hansen, Phys. Rev. Lett. **81**, 4664 (1998).
[3] B. Jakobsen, H. F. Poulsen, U. Lienert, J. Almer, S. Shashtri, H. O. Sorensen, C. Gundlach, and W. Pantleon, Science **312**, 889 (2006).
[4] F. R. N. Nabarro, Mater. Sci. Eng., A **317**, 12 (2001).
[5] R. LeSar and J. M. Rickman, Phys. Rev. B **65**, 144110 (2002).
[6] D. Gomez-Garcia, B. Devincre, and L. P. Kubin, Phys. Rev. Lett. **96**, 125503 (2006).
[7] F. Léonard and R. C. Desai, Phys. Rev. B **58**, 8277 (1998).
[8] S.-B. Lee, J. M. Rickman, and K. Barmak, Acta Mater. **51**, 6415 (2003).
[9] M. Haataja and F. Léonard, Phys. Rev. B **69**, 081201(R) (2004).
[10] Y. Imry and S.-K. Ma, Phys. Rev. Lett. **35**, 1399 (1975).
[11] M. Aizenman and J. Wehr, Phys. Rev. Lett. **62**, 2503 (1989).
[12] J. Bricmont and A. Kupiainen, Phys. Rev. Lett. **59**, 1829 (1987).
[13] T. Nattermann, J. Phys. C **16**, 6407 (1983).
[14] J. Burgy, A. Moreo, and E. Dagotto, Phys. Rev. Lett. **92**, 097202 (2004).
[15] R. Thomson, M. Koslowski, and R. LeSar, Phys. Rev. B **73**, 024104 (2006).
[16] J. P. Hirth and J. Lothe, *Theory of Dislocations* (McGraw-Hill, New York, 1968).
[17] R. J. Amodeo and N. M. Ghoniem, Phys. Rev. B **41**, 6958 (1990).
[18] M.-C. Miguel, A. Vespignani, S. Zapperi, J. Weiss, and J.-R. Grasso, Nature (London) **410**, 667 (2001).
[19] M. Carmen Miguel, A. Vespignani, M. Zaiser, and S. Zapperi, Phys. Rev. Lett. **89**, 165501 (2002).
[20] E. Bittencourt, A. Needleman, M. E. Gurtin, and E. Van der Giessen, J. Mech. Phys. Solids **51**, 281 (2003).
[21] I. Groma, Phys. Rev. B **56**, 5807 (1997).
[22] I. Groma and B. Bako, Phys. Rev. Lett. **84**, 1487 (2000).
[23] I. Groma, G. Györgyi, and B. Kocsis, Phys. Rev. Lett. **96**, 165503 (2006).
[24] F. F. Csikor and I. Groma, Phys. Rev. B **70**, 064106 (2004).
[25] J. M. Rickman, J. Viñals, and R. LeSar, Philos. Mag. **85**, 917 (2005).
[26] A. Gulluoglu, D. J. Srolovitz, R. LeSar, and P. S. Lomdahl, Scr. Metall. **23**, 1347 (1989).
[27] H. Y. Wang, R. LeSar, and J. M. Rickman, Philos. Mag. A **78**, 1195 (1998).
[28] M. Zaiser, M. Carmen Miguel, and I. Groma, Phys. Rev. B **64**, 224102 (2001).
[29] As we are only considering two-dimensional Fourier space, the usual factor of $\delta(q_z)$ is not present in the Fourier transform of the dislocation density.
[30] H. L. Friedman, *A Course in Statistical Mechanics* (Prentice-Hall, Englewood Cliffs, NJ, 1985).
[31] T. E. Faber and J. M. Ziman, Philos. Mag. **11**, 153 (1965).
[32] J. D. Gunton and M. Droz, *Introduction to the Theory of Metastable and Unstable States* (Springer-Verlag, New York, 1983).
[33] T. Mura, *Micromechanics of Defects in Solids*, 2nd ed. (Kluwer, Dordrecht, 1991).